Hydrogen storage behavior of magnesium catalyzed by nickel-graphene nanocomposites

Boris P. Tarasov [a], Artem A. Arbuzov [a], Sergei A. Mozhzhuhin [a],
Aleksei A. Volodin [a], Pavel V. Fursikov [a], Mykhaylo V. Lototskyy [b],
Volodymyr A. Yartys [c,*]

[a] Institute of Problems of Chemical Physics of RAS, Chernogolovka, 142432, Russia
[b] HySA Systems Centre of Competence, South African Institute for Advanced Materials Chemistry, University of the Western Cape, Bellville, 7535, South Africa
[c] Institute for Energy Technology, Kjeller, NO 2027, Norway

ARTICLE INFO

ABSTRACT

In present study nanocomposites of Graphene Like Material (GLM) and nickel containing 5—60 wt % Ni were prepared by a co-reduction of graphite oxide and Ni^{2+} ions. These nanocomposites served as effective catalysts of hydrogenation-dehydrogenation of magnesium based materials and showed a high stability on cycling. Composites of magnesium hydride with Ni/GLM were prepared by high-energy ball milling in hydrogen. The microstructures and phase compositions of the studied materials were characterized by XRD, SEM and TEM showing that Ni nanoparticles have size of 2—5 nm and are uniformly distributed in the composites. The kinetic curves of hydrogen absorption and desorption by the composites were measured using a Sievert's type laboratory setup and were analyzed using the Avraami — Erofeev approach. The re-hydrogenation rate constants and the Avraami exponents fitting the kinetic equations for the $Mg/MgH_2+Ni/GLM$ composites show significant changes as compared to the Mg/MgH_2 prepared at the same conditions and this difference has been assigned to the changes in the mechanism of nucleation and growth and alteration of the rate-limiting steps of the hydrogenation reaction. The composites of Mg with Ni/GLM have a high reversible hydrogen capacity exceeding 6.5 wt % H and also show high rates of hydrogen absorption and desorption and thus belong to the promising hydrogen storage materials.

© 2019 Hydrogen Energy Publications LLC. Published by Elsevier Ltd. All rights reserved.

Introduction

The main focus in the development of the materials for hydrogen energy technologies concerns efficient hydrogen storage materials [1,2] and catalysts for the processes involving molecular hydrogen including catalysts of hydrogenation of various compounds and electrochemical oxidation of hydrogen in fuel cells [3,4].

Magnesium hydride is considered as a promising hydrogen storage material due to its high gravimetric (7.6 wt% H_2) and volumetric (110 g H/L) hydrogen storage capacities. However,

there are several disadvantages that hamper the broad use of magnesium as a hydrogen storage material. Due to the high activation barrier of dissociation of hydrogen molecules and low diffusion rate of hydrogen atoms through the layer of magnesium hydride, the hydrogenation rates are low at temperatures below 350°C. Several approaches have been developed to overcome these drawbacks. These approaches are comprehensively reviewed in Refs. [5—9].

One of the efficient methods of the preparation of magnesium hydride with improved hydrogen sorption performance is mechano-chemical synthesis which includes processing of Mg or MgH_2 by ball milling in inert or hydrogen atmosphere [10,11]. Further improvements can be achieved by introducing various catalytic additives into Mg/MgH_2 [12—18], and/or by a combination of the ball milling of Mg or Mg alloys with other types of processing including rapid solidification [19], equal channel angular pressing [20] or high-pressure torsion [21], as well by providing additional energy inputs to the reactants (plasma-assisted milling [22—24], light activation [25]). In most of the cases the improvements of hydrogenation/dehydrogenation kinetics accompany such a processing while there are also examples of the destabilization of magnesium-based hydrides [22,24] caused by the processing. The improvements are mostly pronounced for the preparation processes which involve high energy reactive ball milling of Mg with the additives performed in hydrogen gas (HRBM); see Refs. [11,15,18] as examples. During HRBM, the formed hydride layer is removed by the mechano-chemical processing consequently providing access of hydrogen gas to the fresh magnesium surface. Thus, synthesized MgH_2 has submicron particle sizes while its surface contains a significant number of induced defects, which notably increases the hydrogenation and dehydrogenation rates.

Various catalytic additives were used during the mechano-chemical synthesis to increase the hydrogenation rate of Mg. As an example, the presence of 3d transition metals (Ni, Nb, Pd, etc.) activates the dissociation of hydrogen molecules [13,26] thereby accelerating the magnesium hydrogenation. Particular attention has been paid to the carbon additives such as graphite, carbon nanotubes, fullerenes and carbon black [23,27—33]. As it has been shown in Ref. [34], carbon nanomaterials can form graphene layers on the magnesium surface which catalyzes the hydrogenation. It is commonly accepted that the effect of graphene has its roots in the fact that graphene layers prevent sintering and grain growth of crystalline Mg and MgH_2 thereby assisting hydrogenation and dehydrogenation processes, and this positive effect remains during hydrogen absorption/desorption cycles. Recent studies [35—37] demonstrated that graphene-like materials can be used as catalytic additives in hydrogenation/dehydrogenation processes. Graphene-like materials form envelopes around magnesium particles and furthermore cause an increase in the rates of hydrogenation/dehydrogenation due to increased thermal conductivity of the composites.

The composites containing nanosized metal clusters deposited on various carbon materials with a high specific surface area belong to the most efficient catalysts [3,4,38—40]. Various types of nanostructured carbon (fullerene black, nanotubes, and nanofibers) show advanced properties in terms of using them as metal catalysts supports, since metal clusters can be deposited on them in a uniform manner and do not agglomerate during the phase transformations thus ensuring the stability of the catalysts.

During the last years, numerous published reference data appeared and showed that graphene and graphene-like materials belong to the promising support materials for the nanostructured metals and metal oxide catalysts [41—48]. However, the structure and properties of the obtained metal graphene composites substantially depend on the preparation processes. As an example, synthesis of the nanostructured $Ni(OH)_2$ proceeds in accordance with different growth mechanisms when it is deposited on graphite oxide (GO) or on reduced GO [49]. Oxygen-containing groups and structure defects which are present in GO cause its interaction with metal salts, which results in a formation of nuclei of the metal clusters formed because of the reduction of metal ions. The reduced GO contains much less functional groups and defects, which contributes to the recrystallization of the Ni clusters and formation of large, well-developed Ni crystallites. Graphene-like materials with deposited metallic nanoparticles can serve as catalysts of various chemical and electrochemical processes. As an example, Pt or Pd nanoparticles deposited on graphene surfaces are used as catalysts during the hydrogenation of unsaturated hydrocarbons and nitrocompounds [50—52] and in the electrocatalytic oxidation [53].
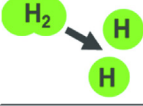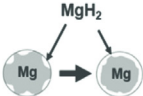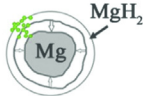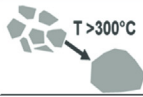
In the present study, we propose a potentially scalable method for obtaining Mg-based hydrogen storage materials which utilizes the key features of these approaches (Fig. 1), including (a) nanoconfinement of Mg particles; (b) use of catalysts of the chemical reactions involving hydrogen; and (c) improvement of the thermal conductivity of hydrogen storage materials in the powder beds.

This work was aimed at the development of an effective method for producing the powder composites of magnesium with nickel-containing graphene-like materials (Ni/GLM), and at studying their hydrogen absorption and desorption behaviors.

Experimental

GO was obtained from natural graphite GK-1 (ash content ≤1 wt%, GOST 4404-78) according to the procedure described in detail in Ref. [54]. GLMs were obtained by thermal reduction of GO in a tubular resistance furnace. Dry GO (10 mg) was placed into a medium part of a quartz reactor under the flow of argon gas (0.2 L/min), while the reactor was heated up to 900°C. In 3—5 s, GO underwent an explosive decomposition to produce gaseous CO, CO_2, and H_2O. The solid product (with considerably increased volume) was removed from the hot zone by argon flow. The obtained powder was annealed in the atmosphere of argon at 900°C for 3 h.

The Ni/GLM composite was prepared by simultaneous reduction of GO and nickel (II) from the mixture prepared separately by freeze drying of GO dispersion in $Ni(CH_3COO)_2$ aqueous solution. For this purpose, the GO aqueous suspension together with the corresponding amount of $Ni(CH_3COO)_2 \cdot 4H_2O$ were processed in an ultrasonic bath for 60 min. The obtained mixture was placed in a 1 L pear-shaped flask and frozen by placing the flask in a Dewar filled with liquid

Sketch	Process stage $Mg + H_2 \leftrightarrow MgH_2$	Problems	Solution
	Hydrogen dissociation	High activation energy of dissociation of the hydrogen molecule	Use a Ni catalyst
	Nucleation and growth of MgH_2	Low reaction rate and heat transfer	Uniform distribution of nanoscale catalyst in Mg. Increased heat transfer due to the use of GLM
	Diffusion of H atoms through a layer of MgH_2	Low diffusion rate of hydrogen through a layer of MgH_2	Obtaining Mg particles with submicron size
	Dehydrogenation of MgH_2	Sintering of Mg particles at high temperatures	Use of GLM to prevent sintering of Mg particles

Fig. 1 — **A sketch presenting the main features of the method proposed in the present study for obtaining Mg-based composite materials with improved hydrogen storage performance.**

nitrogen. Then residual water was removed from the vapors after being equilibrated at ambient conditions, by using a vacuum pump (~$1 \cdot 10^{-3}$ atm) equipped with a nitrogen trap, until the mixture became completely dry. The reduction of the dried mixture was performed for 30 min in a 40 mm tubular reactor at 300—500°C in a flow of hydrogen gas (rate 200 mL/min). The obtained nickel-graphene composites contained from 5 to 60 wt % of Ni nanoparticles.

Hydrogenation of Mg and magnesium-graphene composites was carried out by mechano-chemical processing. The required amount of graphene material, together with 1 g of 0.5—1 mm magnesium powder, and 10 mm steel balls (the sample-to-balls mass ratio was 1/40) were placed into an 80 ml stainless steel vial. The loading was performed in argon glove box. The milling was performed using a Pulverisette 6 planetary ball mill at a rotational speed of 500 rpm in a 4 N pure hydrogen gas with initial hydrogen pressure of 25 atm. The hydrogenation rate was determined by the change of hydrogen pressure measured every hour during the mechano-chemical processing (accuracy 0.2 atm).

The cycling stability of hydrogen storage characteristics of the magnesium composites in hydrogenation-dehydrogenation cycles was studied by performing absorption-desorption experiments using a Sievert's type laboratory setup at the following conditions: (a) The dehydrogenation was carried out at pressure of 1 atm at 350°C; (b) The hydrogenation was performed at a pressure of 5.5 atm at 300°C.

Additional studies of the dehydrogenation kinetics were carried out at different temperatures, from 320 to 350 °C. The H_2 pressures at the beginning and the end of the dehydrogenation were of 1.2 and $\leq$ 1.3 atm, respectively — thus, the experimental conditions were close to isobaric.

The obtained composites were also characterized by a thermogravimetric analysis and using differential scanning calorimetry performed at 30—1000 °C with the linear heating rate of 5 K/min using NETZSCH STA 409C Luxx thermal analyzer. The elemental composition was determined by a Vario Micro cube CHNS/O analyzer. IR spectra were recorded

using a Perkin-Elmer Spectrum 100 Fourier spectrometer in the interval 450—4000 cm^{-1}. Specific surface area was measured by the BET method at liquid nitrogen temperature using SORBI-MS analyzer. The phase composition was investigated on DRON-UM2 and SIEMENS D500 X-ray diffractometers (Cu $K\alpha$ radiation). The microstructure of the materials was studied with a Zeiss LEO SUPRA 25 scanning electron microscope.

The collected data on the hydrogenation, dehydrogenation and re-hydrogenation of the studied samples were processed by a formal kinetics analysis using the Avraami — Erofeev equation:

$$\alpha = A_0 \left\{ 1 - \exp\left[- \left(\frac{t}{t_0} \right)^n \right] \right\} \tag{1}$$

where $\alpha = 0 \dots 1$ is the actual value of Mg→MgH_2 reacted fraction, $A_0 \leq 1$ is the maximum (asymptotic) value of the reacted fraction, t is the time, t_0 is the characteristic reaction time (reciprocal rate constant; t_0 shows the time required to complete the transformation for ~63%), and n is an exponential factor (Avraami exponent) related to the reaction mechanism.

Two complementary mechanisms — Phase Transformation governed by Nucleation and Growth (N&G) and Diffusion-controlled (DC) transformation — were identified as contributing to the mechanism of the hydrogenation in the metal-hydrogen systems [55]. Their contribution is related to the numerical value of the exponential factor n[1]. When Phase

---

[1] From a formal point of view, the Avraami-Erofeev equation is applicable only for the processes which involve nucleation and growth, where the exponential factor (n is an integer having the values between 1 and 4) depends on the nucleation mechanism (random or preferential sites) and the growth dimensionality [55]. However, its applicability for the reactions with integer or half-integer values of $n \geq 0.5$ has been demonstrated as well [57] but these latter process are considered to be diffusion-controlled. Importantly, non-integer values of $n > 1$ can be associated with the change of the nucleation mechanism during the progression of the reaction [56].

Transformation is a rate limiting step, the values of n are between 1 and 4; in contrast, when n is between 0.5 and 1, then the process is diffusion-controlled, and when $1 \leq n \leq 2.5$ the N&G and DC mechanisms cannot be differentiated. From that is can be concluded that for the values of n between 2.5 and 4, only phase transformation contributes via a mechanism of N&G; for the values of n between 0.5 and 1 the process is exclusively controlled by hydrogen diffusion. In turn, for the values of n between 1 and 2.5, the two mechanisms can act in parallel. As an example, for $n = 1$, the mechanism has contributions from both Geometry specified diffusion and Grain boundary nucleation [55].

In practical applications of the Avraami − Erofeev equation, the fitted values of n normally have non-integer values, as shown during mathematical modelling of the reaction kinetics for the hydrogenation of magnesium catalyzed by Ferrovanadium [58].

The best fits for the re-hydrogenation of magnesium-graphene composites was obtained when assuming that the hydrogenation process received contributions from two processes, a fast and a slow hydrogenation processes. This feature is similar to the one observed earlier for the Mg–Ti nanocomposites ball milled in hydrogen gas [18] and was accounted using the following Eq. (2), which is a modified Eq. (1):

$$\alpha = A_1 \left\{ 1 - \exp\left[-\left(\frac{t}{t_1} \right)^{n_1} \right] \right\} + A_2 \left\{ 1 - \exp\left[-\left(\frac{t}{t_2} \right)^{n_2} \right] \right\} \quad (2)$$

where the indexes 1 and 2 correspond to the fast and slow processes, respectively ($t_1 < t_2$), and A_1 and A_2 are the contributions of the processes 1 and 2 to the observed reacted fraction, α.

Results and discussion

During the oxidation of graphite, planar sp^2-hybridized graphene layers turn into a three-dimensional corrugated structure of GO containing sp^3-hybridized carbon atoms. Elemental analysis showed that GO contained 45.9 wt% O, which corresponds to the atomic ratio C/O = 1.5. It is known that carboxylic, epoxy, and hydroxyl groups are removed first during the heat processing of GO in an inert atmosphere, while stable phenolic, cyclic ether, and carbonyl groups are preserved up to 800°C [59]. Rapid heating to 900°C causes GO decomposition associated with a ~30% weight loss of the sample and vigorous evolution of CO, CO_2, and H_2O. The removal of oxygen-containing groups during the thermal reduction took place and was confirmed by elemental analysis and IR spectroscopy. The atomic ratio C/O, which is the measure of an extent of GO reduction, increases to 4.3 as a result of a thermal treatment. An additional annealing in the flow of argon removed most of oxygen-containing groups remaining after the thermal reduction, and the C/O ratio further increased reaching 42.6. The evolution of gases taking place as a result of thermal reduction caused splitting of graphitic layers and prevented their aggregation. As expected, when measured by the BET method, the specific surface area of the obtained GLM was high, 620 m^2/g.

GO can form stable aqueous suspensions containing up to 2 wt % of GO, which allows preparing its composites with water-soluble salts. Oxygen-containing groups and defects cause absence of some carbon atoms in the GO allowing interactions with metal ions and creating growth centers of nanoparticles.

We developed a novel approach to prepare the composites which is described below, $Ni(CH_3COO)_2$ was dissolved in an aqueous suspension of GO, then the liquid suspension was rapidly frozen, and the water was removed by sublimation. This made it possible to avoid the formation of a GO film and the deposition of large $Ni(CH_3COO)_2$ crystals. In contrast to GO films, the obtained composite GO/$Ni(CH_3COO)_2$ was not a subject to the explosive gas release when heated in a flow of hydrogen gas at 300−500 °C, which allowed effective reduction of GO and Ni(II). The processing temperature of 400 °C was found to be optimal for the synthesis of nickel-containing composites, since it provided the most complete reduction of GO and nickel ions. Therefore, in our further studies we used the composites obtained at this temperature.

After the reduction, the atomic ratio C/O increased to 21.2. Depending on the amount of $Ni(CH_3COO)_2$, the obtained composites contained 5 (Ni/GLM-1), 10 (Ni/GLM-2), 15 (Ni/GLM-3), 25 (Ni/GLM-4), and 60 wt % of nickel (Ni/GLM-5). According to the data of scanning electron microscopy (SEM) study (Fig. 2), Ni particles were found to be uniformly distributed over the GLM surface of Ni/GLM composites obtained in such a way. The size of nanoparticles depended on the content of Ni indicating that nucleation and growth mechanism was the case. As an example, the size of Ni nanoparticles was 2−5 nm for Ni/GLM-1 (Fig. 2a) and increased to 100−500 nm for Ni/GLM-5 (Fig. 2d).

Fig. 3a shows the curves of Mg→MgH_2 reaction fraction time dependencies during the mechano-chemical processing. Very good fits were obtained when using the formal kinetics analysis adopted in Eq. (1) (Table 1) to process the collected data. Indeed, Pearson correlation coefficients showed the values exceeding $R^2 = 0.99$ for each set of the processed data. During the milling, the hydrogenation of pure Mg exhibited an S-shaped kinetic curve behavior (Fig. 3a, curve 1). The value of the Avraami exponent $n = 4$ corresponded to the random nucleation and 3D-growth reaction mechanism [55,56].

The reaction rate was rather slow (characteristic time was about 5 h) which can be related to a slow nucleation rate during the hydrogenation. The hydrogenation rate increased after 7 h of mechano-chemical processing, since brittle MgH_2 accumulating in the course of the milling was easily removed from the metal particles thus exposing an active to hydrogen fresh Mg surface.

In contrast, the hydrogenation of magnesium composite containing 10 wt % of GLM (Fig. 3a, curve 2) proceeds with >2 times shorter characteristic times; the rate of hydrogenation further increased with the increase of the GLM content. The Avraami exponent decreased to $n \sim 1.7$. According to Ref. [60], the decrease of Avraami exponent may have its origin in the limitations associated with the possible nucleation regions when the nucleation proceeds at points ($n = 3$), edges ($n = 2$) or at surfaces ($n = 1$). Furthermore, non-integer values of n can be associated with the contribution of diffusion [57], and/or the change of the nucleation mechanism during the reaction [55]. In any case, addition of GLM resulted in the
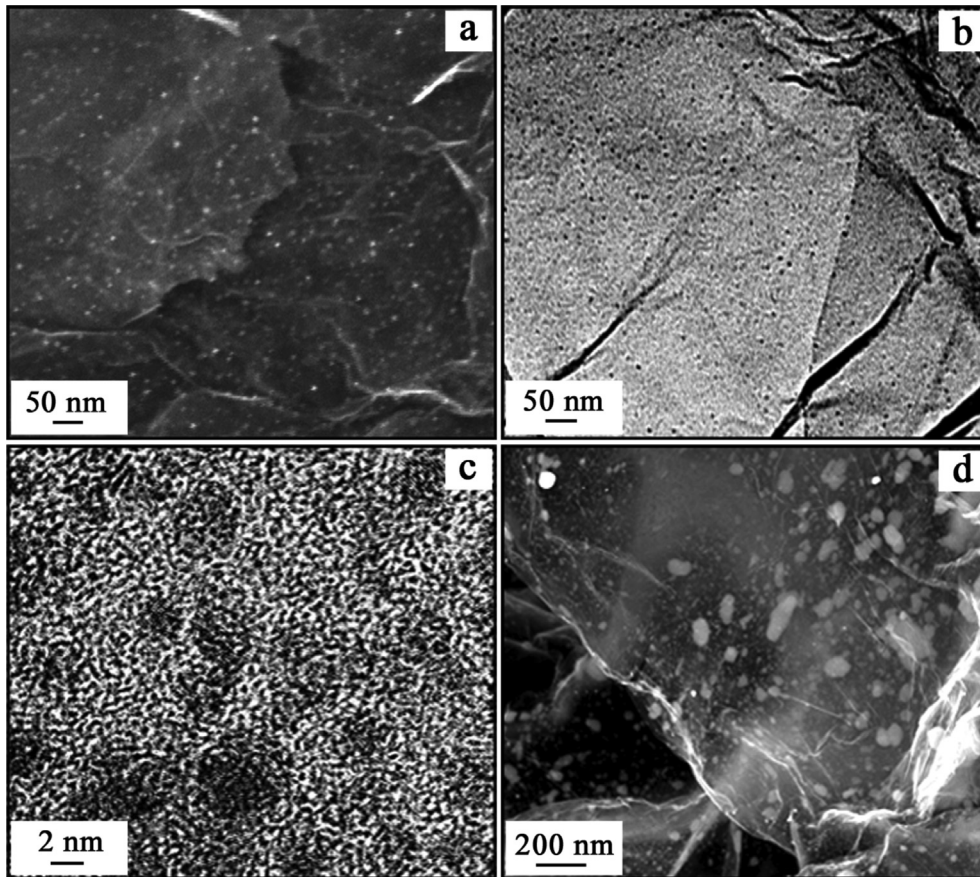
Fig. 2 – SEM (a) and TEM (c, d) images of the catalyst Ni/GLM-1 (5 wt% Ni deposited on GLM); SEM image (b) of the catalyst Ni/GLM-5 (60 wt% Ni deposited on GLM).

change of the reaction mechanism (see Fig. 3a). This means that despite of the existing limitation of the nucleation regions upon addition of GLM, the nuclei formed faster, and their number was high enough to provide the increase in the overall reaction rate already at the beginning of the transformation [55].

We note that although the Avraami-Erofeev equation was successfully used in a number of studies [16,18,22,23,55] for the modelling of kinetics of hydrogenation and dehydrogenation of Mg-based hydrogen storage materials, it is impossible to make an unambiguous conclusion about the reaction mechanism based on the value of Avraami exponent only in
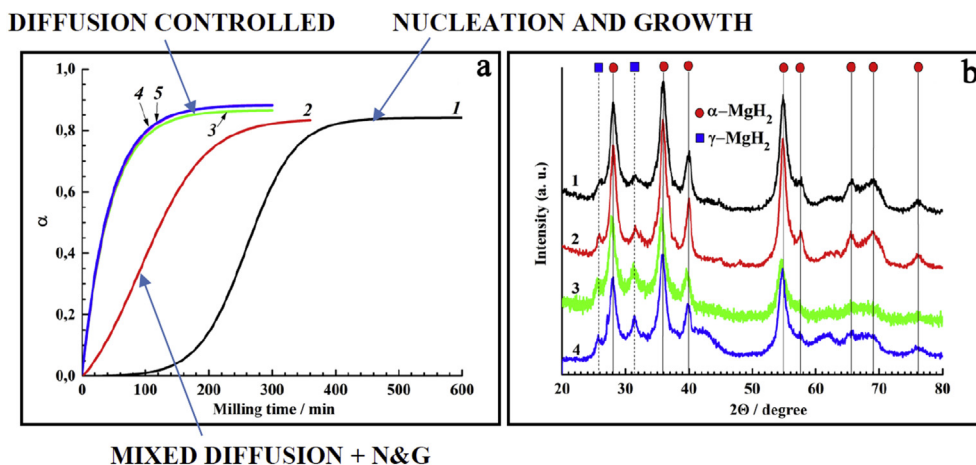

Fig. 3 – a: Curves of Mg hydrogenation without GML (1) and with 10 wt% of GLM (2), Ni/GLM-2 (3), Ni/GLM-3 (4), and Ni/GLM-4 (5) during the mechano-chemical processing; b: X-ray diffraction patterns of MgH$_2$ (1) and composites containing 1 (2) and 10 wt% of GLM (3) and 10 wt% of Ni/GLM-4 (4).

Table 1 – Results of the refinements of the kinetic data of the hydrogenation process (Fig. 3a) when using Eq.1.

Curve #	Sample	Fitting parameters and their standard deviations			R^2
		A_0	t_0 [min]	n	
1	Mg (no GLM)	0.8362 (9)	282.9 (3)	4.00 (2)	0.99789
2	10% GLM	0.8397 (4)	131.4 (1)	1.668 (3)	0.99962
3	10% Ni/GLM-2	0.866760 (2)	43.7686 (5)	1.00174 (2)	1
4	10% Ni/GLM-3	0.883440 (2)	44.2050 (5)	1.00099 (2)	1
5	10% Ni/GLM-4	0.882240 (3)	43.1160 (6)	1.00038 (2)	1

case it is in the range between 1 and 2.5. As it was shown in Ref. [57], at $1 \leq n \leq 2.5$ the rates of H_2 absorption/desorption can be limited by both diffusion and phase transformation and thus a mixed mechanism is likely to be the case.

For both undoped Mg and Mg–GLM composites, the hydrogenation virtually stopped at $\alpha \approx 0.84$ and did not reached a completion. The reason for that is in a very slow H diffusion through the growing MgH_2 layer and thus the diffusion becomes a rate-limiting step of the hydrogenation at the end of the reaction. We note that the observed maximum value of the reacted fraction was higher than it was achieved for the hydrogenation of Mg in "static" conditions, without the ball milling ($\alpha \approx 0.75$ at T~250 °C) [61].

In contrast, reactive ball milling of individual magnesium metal in H_2 resulted in a formation of stoichiometric MgH_2 ($\alpha = 1$) [62]. The differences in the results obtained in the present study and in the reference work can be explained by the difference of the experimental conditions, first of all, in use of a coarser Mg powder (0.5–1 mm) in this work as compared to the magnesium powder utilized in Ref. [62] (0.1–0.3 mm).

There are several reasons helping to explain the increased hydrogenation rate due to the doping by GLM. GLM, like other carbon materials described in earlier studies, covers the surface of the magnesium particles during the mechanochemical processing thus preventing their agglomeration and serving as a hydrogen carrier along the Mg(MgH_2)-C interphase boundary [34].

Adding Ni/GLM-2 composite to magnesium (Fig. 3a, curve 3) substantially increases the rate of Mg hydrogenation due to the high catalytic activity of Ni nanoparticles causing easy dissociation of H_2 molecules, while the coating of MgH_2 fine particles by the GLM preserves their submicron size obtained during MgH_2 dehydrogenation and provides high thermal conductivity of Mg/MgH_2+Ni/GLM composites. At the same time, the increase of Ni content to 15 and 25 wt % in the composite (Fig. 3a, curves 4 and 5) does not notably affect the hydrogenation rate and only slightly increases the reacted fraction. The composites doped by Ni/GLM show close values of kinetic parameters of the hydrogenation (Table 1), with maximum reacted fraction of 0.87–0.88, characteristic reaction time around 45 min, or ~3 times shorter than for Mg/MgH_2+GLM composite, and Avraami exponent value equal to 1, indicating that a grain boundary nucleation [57,60] was the case.

The DSC curve of MgH_2 decomposition shows appearance of one broad peak centered at 400°C (Fig. 4). When adding GLM, two endothermic peaks appear in the decomposition curves that indicates presence of two phases: γ-MgH_2 and α-MgH_2.

The peak on the DSC curve for the γ-phase is shifted by 20°C towards the lower temperatures as compared to the α-phase for MgH_2/1% GLM, and by 50°C for MgH_2/5% GLM. The reduced stability of the thermodynamically unstable γ-MgH_2 has been reported earlier during *in situ* SR XRD study of hydrogen desorption from a mixture of γ-MgH_2 and α-MgH_2 obtained by reactive ball milling of Mg in hydrogen [62].

The presence of a metastable γ-dihydride MgH_2 was confirmed by XRD data: its X-ray diffraction peaks are clearly visible in Fig. 3b. In all X-ray diffraction patterns, the peak positions for both hydride phases are in good agreement with the data reported in Ref. [62]: α-MgH_2 (tetragonal; $a = 0.4515$ nm, $c = 0.3019$ nm) and γ-MgH_2 (orthorhombic; $a = 0.4526$ nm, $b = 0.5448$ nm, $c = 0.4936$ nm).

The content of γ-MgH_2 grows together with the content of GLM in the as-synthesized composites (Fig. 3b, curves 2 and 3; Fig. 5b, curve 1). As expected, this metastable (at normal conditions) modification of MgH_2 is not present in the subsequent dehydrogenation-hydrogenation cycles (Fig. 5b, curve 2). The particle size of magnesium hydride in the obtained composites ranges from 500 nm to several microns (Fig. 5a).

Selected data of the dehydrogenation of mechanochemically prepared MgH_2-containing composites carried out at pressure of 1 atm at 350°C are presented in Fig. 6a and Table 2. The 80% dehydrogenation for both MgH_2 (Fig. 6a, curve 1) and the composites (Fig. 6a, curves 2 and 3) was achieved in the first 10 min, and the composites demonstrated higher transformation rates at the beginning of the
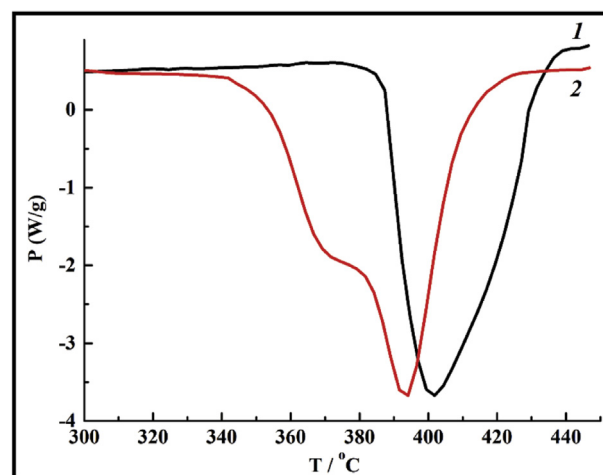
Fig. 4 – DSC profiles obtained in argon flow when applying the linear heating rate of 5 K/min to MgH_2 (1) and MgH_2 + 1 % wt of GLM (2).
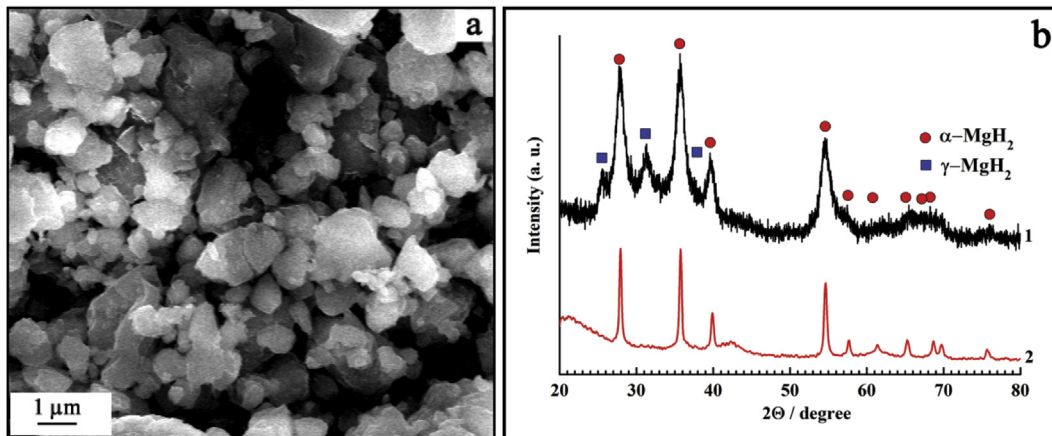
Fig. 5 − SEM image (a) and X-Ray diffraction pattern (b) of the as-prepared MgH₂+10% (11% Ni/GLM) composite (1) and the composite after accomplishing ten absorption-desorption cycles (2).
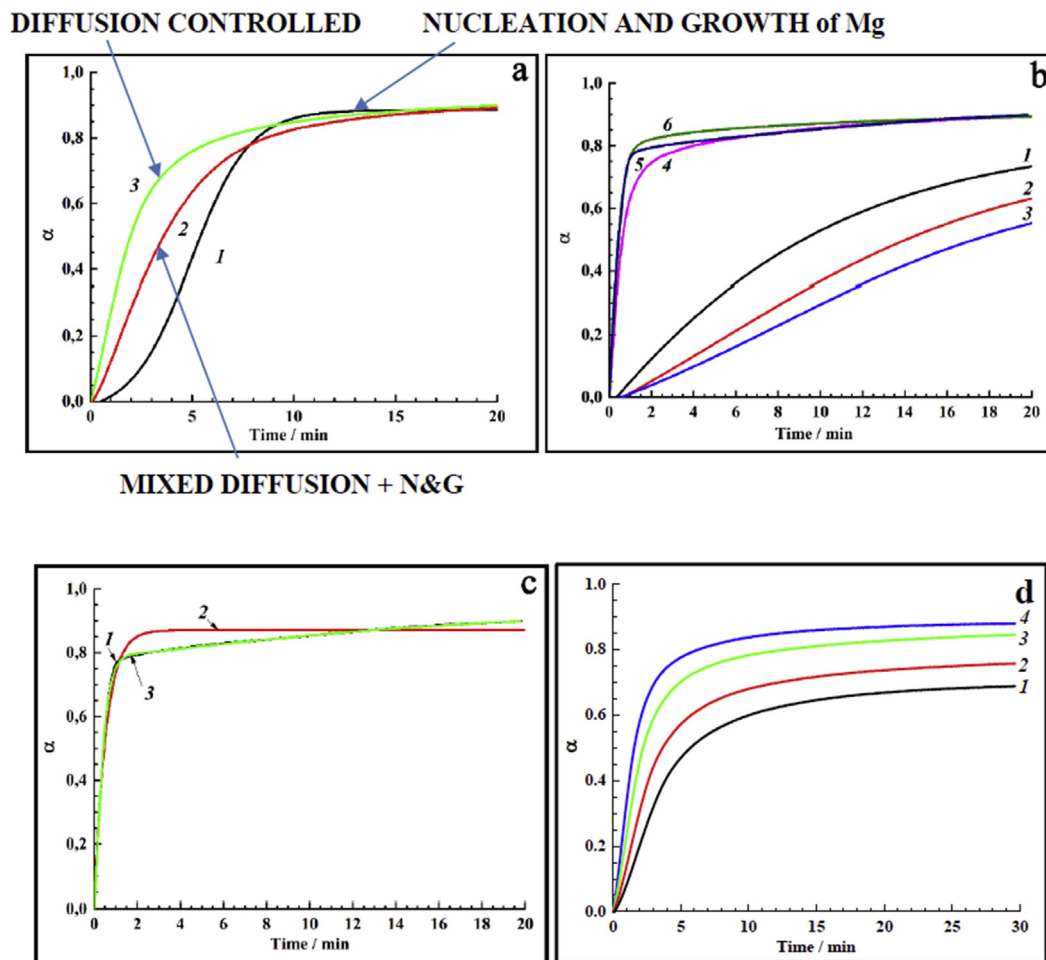

Fig. 6 − a: Curves of dehydrogenation of MgH₂ for individual MgH₂ (1) and for MgH₂ containing 10 wt% of GLM (2), and Ni/GLM-4 (3); b: Curves of hydrogen absorption for Mg (1−3) and the composite with 10 wt% of Ni/GLM-4 (4−6) during the first (1,4), fifth (2,5), and tenth (3,6) hydrogenation cycles; c: hydrogen absorption by the composite containing 10 wt% of Ni/GLM-4 during the tenth hydrogenation cycle; experimental data (1) and results of their fitting with Eq. (1) (2) and Eq. (2) (3); d:Curves of dehydrogenation of MgH₂ for the composite with 10 wt% of Ni/GLM-3 at the temperature of 320 (1), 330 (2), 340 (3) and 350 °C (4).

Table 2 — Results of the refinements of the dehydrogenation kinetics data (Fig. 6a) using Eq. 1					
Curve #	Sample	Fitted parameters			R^2
		A_0	t_0 [min]	n	
1	MgH$_2$	0.8836 (2)	5.817 (2)	2.520 (3)	0.99983
2	10% GLM	0.8820 (4)	4.22 (1)	1.241 (3)	0.99887
3	10% Ni/GLM-4	0.8847 (6)	2.507 (9)	0.962 (5)	0.99355

dehydrogenation. Introduction of GLM and Ni/GLM causes changes of the kinetic parameters of dehydrogenation (see Table 2) similar to the changes observed for the hydrogenation during the ball milling (Table 1).

The fitted value of n ~ 2.5 for the non-modified Mg indicated that the nucleation and growth mechanism remained valid. The mechanism transforms into the process with a zero order nucleation rate for Mg/MgH$_2$+GLM (n ~ 1.25) and a grain boundary nucleation for Mg/MgH$_2$+Ni/GLM (n ~ 1) (see Fig. 6a). For the two latter processes a contribution from the diffusion as a factor limiting the overall rate of the processes is very likely, as suggested in Ref. [57]. The characteristic reaction time becomes very short, below 6 min for the undoped Mg; the doping by GLM shortens it by ~30% followed by a further shortening in ~1.7 times upon modification with Ni/GLM.

Magnesium particles become sintered during the MgH$_2$ dehydrogenation forming agglomerates which substantially deteriorates kinetics of hydrogen absorption during the subsequent hydrogenation cycles (Fig. 6b, curves 1—3). As it can be seen from Table 3, the cycling results in the drop of the maximum reacted fraction during the transformation of Mg into MgH$_2$, from >0.8 to ~0.75 (as it was mentioned earlier, this is a typical value for the hydrogenation of Mg at lower temperatures when MgH$_2$ is not subjected to the ball milling [61]) throughout ten dehydrogenation − re-hydrogenation cycles. The characteristic reaction time and the Avraami exponent value both increase − from ~9 to >15 min and from ~1.2 to ~1.4, respectively.

Table 3 — Results of the refinements of the re-hydrogenation kinetic data for the undoped Mg (Fig. 6b, curves 1—3) with Eq. (1).					
Curve #	Cycle #	Fitting parameters			R^2
		A_0	t_0 [min]	n	
1	1	0.805 (1)	9.40 (2)	1.161 (2)	0.99964
2	5	0.777 (2)	13.74 (5)	1.384 (3)	0.99969
3	10	0.741 (2)	15.98 (5)	1.428 (2)	0.99984

As mentioned above, GLM layers cover magnesium hydride particles during the mechano-chemical processing thereby preventing their agglomeration during the dehydrogenation. Due to this, and because of a catalytic effect of Ni nanoparticles, the rate of hydrogen absorption is very high during the first and subsequent re-hydrogenation cycles (Fig. 6b, curves 4—6). The maximum reacted fraction increases to 0.92−0.95 (A_1+A_2 in Table 4), and the 80% hydrogenation of Mg is achieved in just 2−4 min.

As it was mentioned earlier, the best fit of the experimental kinetic data for Mg/MgH$_2$+Ni/GLM was achieved assuming that the hydrogenation involves two steps, fast and slow (Eq. (2)). An example of the comparison of the fitting of the experimental data using Eqs. (1) and (2) (Fig. 6c) clearly shows the improvements achieved when using Eq. (2). We note that the observed trends of the change of the re-hydrogenation kinetic parameters for the studied samples are similar to the ones for MgH$_2$−TiH$_2$ nanocomposites prepared by ball milling of Mg + Ti in H$_2$ [18]. Accomplishment of ten dehydrogenation − re-hydrogenation cycles results in a gradual decrease in the contribution of the slow stage ($\frac{A_2}{A_1+A_2}$) with a simultaneous shortening of the characteristic reaction time for the fast stage (from ~36 to ~24 s) and the increase of the characteristic reaction time (from ~5 to ~15 min) for the slow one. The values of the Avraami exponent for the fast stage do not significantly change during the cycling (n ~ 1.3) while the slow stage exhibits the increase of n from ~0.5 (diffusion-controlled process) to ~1.2 (mixed diffusion-controlled and of nucleation and growth mechanisms).

Fig. 6d shows kinetic curves of MgH$_2$ dehydrogenation for the composite with 10 wt% of Ni/GLM-3 taken at four different temperatures in the range of 320−340 °C. The rate constants, K, calculated from the fitted values of t_0 = 1/K using Eq. (1) are presented in Table 5.

The linear fitting of ln K versus 1/T [K] (Fig. 7) yields the value of the activation energy of dehydrogenation of 75 kJ mol H$_2^{-1}$. However, we note that the values of K which were retrieved from a series of isobaric experiments do not take into account the pressure-dependent driving force (PDF) which depends on the temperature-dependent equilibrium H$_2$

Table 4 — Results of the refinement of the re-hydrogenation kinetic data for Mg doped by *Ni/GLM* (Fig. 6b, *curves 4—6*) *with* Eq. (2).									
Curve #	Cycle #	Fitting parameters						A_1+A_2	$\frac{A_2}{A_1+A_2}$	R^2
		Fast stage			Slow stage					
		A_1	t_1 [min]	n_1	A_2	t_2 [min]	n_2			
4	1	0.647 (7)	0.566 (1)	1.215 (8)	0.270 (8)	5.4 (1)	0.68 (2)	0.92	0.29	0.99968
5	5	0.764 (3)	0.474 (1)	1.33 (1)	0.188 (7)	14.3 (9)	0.50 (2)	0.95	0.20	0.99972
6	10	0.7860 (8)	0.422 (1)	1.261 (3)	0.148 (4)	14.8 (4)	1.24 (3)	0.93	0.16	0.99937

Table 5 – Experimental conditions and dehydrogenation rate constants for the composite with 10 wt% of Ni/GLM-3.

Curve # (Fig. 6d)	T [°C]	K [min^{-1}]	P_D [atm]	PDF(T)/PDF (T = 350 °C) (Eq. (3))[a]	K(corr) [min^{-1}]
1	320	0.3359	3.10	0.62	0.2089
2	330	0.4196	3.98	0.76	0.3196
3	340	0.5342	5.07	0.89	0.4739
4	350	0.7054	6.41	1.00	0.7054

[a] $P = 1.25$ atm.

Table 6 – Activation energies for the dehydrogenation of MgH_2.

Material	E_A [kJ mol H$_2^{-1}$]	Reference
Pure MgH_2	160.0	[63]
MgH_2 after 2 h milling	158.5	[64]
MgH_2 + 10% $NiCl_2$	121.3	[64]
MgH_2 + 10% $CoCl_2$	102.6	[64]
$Mg_{95}In_5$ + 12.9% MgF_2	127.7	[22]
$Mg_{85}In_5Al_5Ti_5$ + 7% MgF_2	125.2	[24]
$Mg_{90}In_5Y_5$	147.4	[65]
$Mg_{80}Ce_{18}Ni_2$	63.3	[16]
Mg_3Ce	103.7	[16]
MgH_2 + 10% Ni/GLM-3	76/124.2[a]	This work

[a] With corrections correctly accounting effect of pressure driving force.
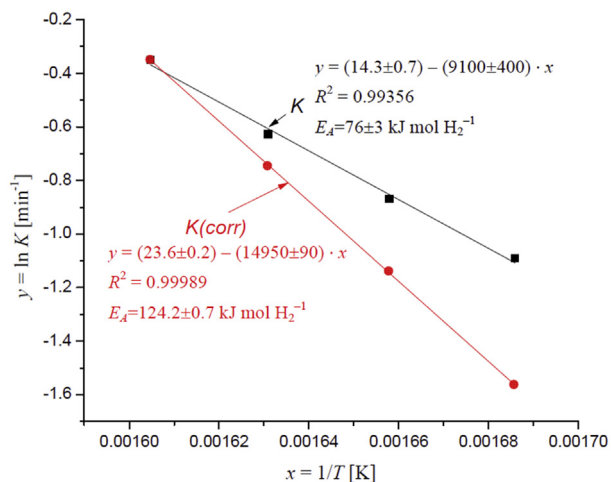
pressure, P_D (apart from the actual H_2 pressure, P). For the diffusion-controlled dehydrogenation reactions that is the case for the studied material (see Fig. 6a, curve 3), Rudman [57] proposed use of the following equation:

$$PDF = T\left[1 - \left(\frac{P}{P_D}\right)^{\frac{1}{2}}\right] \qquad (3)$$

The values of corrected rate constants, $K(corr) = K\left[\frac{PDF(T)}{PDF(T=350°C=623.15\,K)}\right]$, are presented in the last column of Table 5. The Arhenius plot for these values (see Fig. 7) yields the value of dehydrogenation activation energy of 124.2 kJ mol H$_2^{-1}$ (we note that this value should be considered as describing the data in the best possible way because of the higher value of goodness of the fit).

Table 6 presents comparison of the data on the activation energy of MgH_2 dehydrogenation determined in this work (last row) and selected reference data. Since not all of the reference works specify whether the pressure driving force was or was not taken into account in the determination of the rate constant at different temperatures, we include in Table 6 the values of E_A calculated from both original (K) and corrected (K (corr)) values of the rate constants (Table 5, Fig. 7). In both cases the values of MgH_2 dehydrogenation activation energies for MgH_2 prepared by co-milling of Mg with Ni/GLM in hydrogen atmosphere were found to be significantly lower than the corresponding values for pure MgH_2 [63] (the

correction for the pressure driving force has also been introduced in this work). The improvements of the dehydrogenation kinetics observed in our study well agree with the observations of other researchers who reported influence of catalytic additives on the H storage performance of MgH_2 (see Table 6).

Summarising the presented results, we conclude that composites of Mg with 5–10 wt % of Ni/GLM are promising hydrogen storage materials with a high reversible hydrogen storage capacity (>6.5 wt%) and fast dehydrogenation – re-hydrogenation kinetics remaining stable throughout at least ten H_2 desorption – absorption cycles.

Conclusions

A novel method allowing to produce nickel-graphene composites containing nanosized Ni particles uniformly distributed over the GLM surface has been developed. The composites are effective catalysts of the hydrogenation of magnesium. The composites of Mg with Ni/GLM are promising hydrogen storage materials showing a high reversible hydrogen capacity exceeding 6.5 wt % H.

Adding GLM and Ni/GLM significantly improves the kinetics of the formation of MgH_2 during the ball milling in hydrogen gas, as well as dehydrogenation of MgH_2 and, particularly, improves the rates of re-hydrogenation of the ball milled material. The reaction rate constant increases in more than 2 and 6.5 times for the hydrogenation of Mg doped by GLM and Ni/GLM, respectively, as compared to Mg without additives. The corresponding increase in the dehydrogenation rate constant is in 1.4 and 2.3 times. Finally, the re-hydrogenation rate constant for the Mg/MgH$_2$+Ni/GLM composites is 15–37 times higher than the one for the individual Mg/MgH$_2$ prepared at the same conditions. For all studied reactions the doping also results in the significant decrease of the Avraami exponent indicating that limitation of nucleation regions (but with the faster nucleation) is the case and a contribution of H diffusion becomes a rate-limiting step.

Addition of Ni/GLM also improves the cyclic stability of the material providing fast and almost complete re-hydrogenation throughout at least ten dehydrogenation – re-hydrogenation cycles. It was also found that for the Mg/

Fig. 7 – Arhenius plots for the dehydrogenation of MgH_2 for the composite with 10 wt% of Ni/GLM-3.

MgH_2+Ni/GLM composites the re-hydrogenation proceeds via two steps, fast and slow ones, similar to the behavior earlier observed for Mg/MgH_2+TiH_2 composites. During the cycling, the contribution of the slow process into the re-hydrogenation kinetics decreases without a decrease in the maximum hydrogen absorption capacity.

Acknowledgements

REFERENCES

[1] Tarasov BP, Lototskii MV, Yartys VA. Problem of hydrogen storage and prospective uses of hydrides for hydrogen accumulation. Russ J Gen Chem 2007;77:694–711. https://doi.org/10.1134/S1070363207040329.

[2] Tarasov BP. Metal-hydride accumulators and generators of hydrogen for feeding fuel cells. Int J Hydrog Energy 2011;36:1196–9. https://doi.org/10.1016/j.ijhydene.2010.07.002.

[3] Kushch SD, Kujunko NS, Tarasov BP. Platinum nanoparticles on carbon nanomaterials with graphene structure as hydrogenation catalysts. Russ J Gen Chem 2009;79:706–10. https://doi.org/10.1134/S1070363209040057.

[4] Kushch SD, Kuyunko NS, Tarasov BP. Preparation of hydrogenation catalysts based on platinum nanoparticles supported on carbon nanomaterials. Kinet Catal 2009;50:860. https://doi.org/10.1134/S0023158409060093.

[5] Crivello J-C, Denys RV, Dornheim M, Felderhoff M, Grant DM, Huot J, et al. Mg based compounds for hydrogen and energy storage. Appl Phys Mater Sci Process 2016;122(2):85. https://doi.org/10.1007/s00339-016-9601-1.

[6] Crivello J-C, Dam B, Denys RV, Dornheim M, Grant DM, Huot J, et al. Review of magnesium hydride-based materials: development and optimization. Appl Phys Mater Sci Process 2016;122(2):97. https://doi.org/10.1007/s00339-016-9602-0.

[7] Sun Y, Shen C, Lai Q, Liu W, Wang D-W, Aguey-Zinsou K-F. Tailoring magnesium based materials for hydrogen storage through synthesis: current state of the art. Energy Storage Mater 2018;10:168–98. https://doi.org/10.1016/j.ensm.2017.01.010.

[8] Zhang J, Yan S, Qu H. Recent progress in magnesium hydride modified through catalysis and nanoconfinement. Int J Hydrog Energy 2018;43:1545–65. https://doi.org/10.1016/j.ijhydene.2017.11.135.

[9] Yartys VA, Lototskyy MV, Akiba E, Albert R, Antonov VE, Ares JR, et al. Magnesium based materials for hydrogen based energy storage: past, present and future. Int J Hydrog Energy 2019;44:7809–59. https://doi.org/10.1016/j.ijhydene.2018.12.212.

[10] Zaluska A, Zaluski L, Ström-Olsen JO. Nanocrystalline magnesium for hydrogen storage. J Alloy Compd 1999;288:217–25. https://doi.org/10.1016/S0925-8388(99)00073-0.

[11] Huot J, Ravnsbæk DB, Zhang J, Cuevas F, Latroche M, Jensen TR. Mechano-chemical synthesis of hydrogen storage materials. Prog Mater Sci 2013;58:30–75. https://doi.org/10.1016/j.pmatsci.2012.07.001.

[12] Oelerich W, Klassen T, Bormann R. Comparison of the catalytic effects of V, V_2O_5, VN, and VC on the hydrogen sorption of nanocrystalline Mg. J Alloy Compd 2001;322:L5–9.

[13] Hanada N, Ichikawa T, Fujii H. Catalytic effect of nanoparticle 3d-transition metals on hydrogen storage properties in magnesium hydride MgH_2 prepared by mechanical milling. J Phys Chem B 2005;109(15):7188–94.

[14] Zhu M, Wang H, Ouyang LZ, Zeng MQ. Composite structure and hydrogen storage properties in Mg-base alloys. Int J Hydrog Energy 2006;31:251–7.

[15] Lototsky MV, Denys RV, Yartys VA. Combustion-type hydrogenation of nanostructured Mg-based composites for hydrogen storage. Int J Energy Res 2009;33:1114–25. https://doi.org/10.1002/er.1604.

[16] Ouyang LZ, Yang XS, Zhu M, Liu JW, Dong HW, Sun DL, et al. Enhanced hydrogen storage kinetics and stability by synergistic effects of in situ formed $CeH_{2.73}$ and Ni in $CeH_{2.73}$-MgH_2-Ni nanocomposites. J Phys Chem C 2014;118(15):7808–20. https://doi.org/10.1021/jp500439n.

[17] Zhou C, Fang ZZ, Bowman Jr RC. Stability of catalyzed magnesium hydride nanocrystalline during hydrogen cycling. Part I: kinetic analysis. J Phys Chem C 2015;119:22261–71.

[18] Lotoskyy M, Denys R, Yartys VA, Eriksen J, Goh J, Nyallang Nyamsi S, et al. An outstanding effect of graphite in nano-MgH_2–TiH_2 on hydrogen storage performance. J Mater Chem A 2018;6:10740–54.

[19] Wu Y, Lototsky MV, Solberg JK, Yartys VA. Microstructural evolution and improved hydrogenation–dehydrogenation kinetics of nanostructured melt-spun Mg–Ni–Mm alloys. J Alloy Comp 2011;509S:S640–5.

[20] Chiu C, Huang S-J, Chou T-Y, Rabkin E. Improving hydrogen storage performance of AZ31 Mg alloy by equal channel angular pressing and additives. J Alloy Compd 2018;743:437–47.

[21] Hongo T, Edalati K, Arita M, Matsuda J, Akiba E, Horita Z. Significance of grain boundaries and stacking faults on hydrogen storage properties of Mg_2Ni intermetallics processed by high pressure torsion. Acta Mater 2015;92:46–54.

[22] Ouyang LZ, Cao ZJ, Wang H, Liu JW, Sun DL, Zhang QA, Zhu M. Enhanced dehydriding thermodynamics and kinetics in Mg(In)–MgF_2 composite directly synthesized by plasma milling. J Alloy Compd 2014;586:113–7.

[23] Ouyang L, Cao Z, Wang H, Hu R, Zhu M. Application of dielectric barrier discharge plasma-assisted milling in energy storage materials — a review. J Alloy Compd 2017;691:422–35.

[24] Cao Z, Ouyang L, Wua Y, Wang H, Liu J, Fang F, et al. Dual-tuning effects of In, Al, and Ti on the thermodynamics and kinetics of $Mg_{85}In_5Al_5Ti_5$ alloy synthesized by plasma milling. J alloys Compd 2015;623:354–8.

[25] Sun Y, Aguey-Zinsou K-F. Light-activated hydrogen storage in Mg, LiH and $NaAlH_4$. ChemPlusChem 2018;83(10):904–8. https://doi.org/10.1002/cplu.201800190.

[26] Fursikov PV, Tarasov BP. Hydrogen sorbing magnesium alloys and composites. Russ Chem Bull 2018;67:193–9. https://doi.org/10.1007/s11172-018-2058-y.

[27] Lukashev RV, Klyamkin SN, Tarasov BP. Preparation and properties of hydrogen-storage composites in the MgH_2-C system. Inorg Mater 2006;42:726–32. https://doi.org/10.1134/S0020168506070077.

[28] Ranjbar A, Ismail M, Guo ZP, Yu XB, Liu HK. Effects of CNTs on the hydrogen storage properties of MgH_2 and MgH_2-BCC composite. Int J Hydrog Energy 2010;35:7821–6. https://doi.org/10.1016/j.ijhydene.2010.05.080.

[29] Singh MK, Bhatnagar A, Pandey SK, Mishra PC, Srivastava ON. Experimental and first principle studies on hydrogen desorption behavior of graphene nanofibre catalyzed MgH_2. Int J Hydrog Energy 2017;42:960–8. https://doi.org/10.1016/j.ijhydene.2016.09.210.

[30] Xie X, Chen M, Liu P, Shang J, Liu T. High hydrogen desorption properties of Mg-based nanocomposite at moderate temperatures: the effects of multiple catalysts in situ formed by adding nickel sulfides/graphene. J Power Sources 2017;371:112–8. https://doi.org/10.1016/j.jpowsour.2017.10.054.

[31] Liu W, Setijadi E, Crema L, Bartali R, Laidani N, Aguey-Zinsou KF, et al. Carbon nanostructures/Mg hybrid materials for hydrogen storage. Diam Relat Mater 2018;82:19–24. https://doi.org/10.1016/j.diamond.2017.12.003.

[32] Peng D, Ding Z, Zhang L, Fu Y, Wang J, Li Y, et al. Remarkable hydrogen storage properties and mechanisms of the shell–core MgH_2@carbon aerogel microspheres. Int J Hydrog Energy 2018;43:3731–40. https://doi.org/10.1016/j.ijhydene.2018.01.004.

[33] Chen M, Xie X, Liu P, Liu T. Facile fabrication of ultrathin carbon layer encapsulated air-stable Mg nanoparticles with enhanced hydrogen storage properties. Chem Eng J 2018;337:161–8. https://doi.org/10.1016/j.cej.2017.12.087.

[34] Lototskyy M, Sibanyoni JM, Denys RV, Williams M, Pollet BG, Yartys VA. Magnesium–carbon hydrogen storage hybrid materials produced by reactive ball milling in hydrogen. Carbon 2013;57:146–60. https://doi.org/10.1016/j.carbon.2013.01.058.

[35] Liu G, Wang Y, Xu C, Qiu F, An C, Li L, et al. Excellent catalytic effects of highly crumpled graphene nanosheets on hydrogenation/dehydrogenation of magnesium hydride. Nanoscale 2013;5:1074–81. https://doi.org/10.1039/C2NR33347C.

[36] Tarasov BP, Arbuzov AA, Mozhzhuhin SA, Volodin AA, Fursikov PV. Composite materials with 2D graphene structures: applications for hydrogen energetics and catalysis with hydrogen participation. J Struct Chem 2018;59:830–8. https://doi.org/10.1134/S0022476618040121.

[37] Ouyang LZ, Cao ZJ, Li LL, Wang H, Liu JW, Min D, et al. Enhanced high-rate discharge properties of $La_{11.3}Mg_{6.0}Sm_{7.4}Ni_{61.0}Co_{7.2}Al_{7.1}$ with added graphene synthesized by plasma milling. Int J Hydrog Energy 2014;39:12765–72.

[38] Lukashev RV, Klyamkin SN, Tarasov BP. MgH_2-carbon composites for hydrogen storage. In: Veziroglu TN, editor. Hydrogen materials science and chemistry of carbon nanomaterials; 2007. p. 193–9. https://doi.org/10.1007/978-1-4020-5514-0_24.

[39] Tarasov BP, Muradyan VE, Volodin AA. Synthesis, properties, and examples of the use of carbon nanomaterials. Russ Chem Bull 2011;60:1261–73. https://doi.org/10.1007/s11172-011-0194-8.

[40] Fu T, Li Z. Review of recent development in Co-based catalysts supported on carbon materials for Fischer–Tropsch synthesis. Chem Eng Sci 2015;135:3–20. https://doi.org/10.1016/j.ces.2015.03.007.

[41] Tkachev SV, Buslaeva EY, Gubin SP. Graphene: a novel carbon nanomaterial. Inorg Mater 2011;47:1–10. https://doi.org/10.1134/S0020168511010134.

[42] Obraztsov AN, Obraztsova EA, Tyurnina AV, Zolotukhin AA. Chemical vapor deposition of thin graphite films of nanometer thickness. Carbon 2007;45:2017–21. https://doi.org/10.1016/j.carbon.2007.05.028.

[43] Agnoli S, Granozzi G. Second generation graphene: opportunities and challenges for surface science. Surf Sci 2013;609:1–5. https://doi.org/10.1016/j.susc.2012.11.016.

[44] Li F, Jiang X, Zhao J, Zhang S. Graphene oxide: a promising nanomaterial for energy and environmental applications. Nanomater Energy 2015;16:488–515. https://doi.org/10.1016/j.nanoen.2015.07.014.

[45] Tjong SC. Recent progress in the development and properties of novel metal matrix nanocomposites reinforced with carbon nanotubes and graphene nanosheets. Mater Sci Eng R Rep 2013;74:281–350. https://doi.org/10.1016/j.mser.2013.08.001.

[46] Navalon S, Dhakshinamoorthy A, Alvaro M, Garcia H. Metal nanoparticles supported on two-dimensional graphenes as heterogeneous catalysts. Coord Chem Rev 2016;312:99–148. https://doi.org/10.1016/j.ccr.2015.12.005.

[47] Axet MR, Dechy-Cabaret O, Durand J, Gouygou M, Serp P. Coordination chemistry on carbon surfaces. Coord Chem Rev 2016;308:236–345. https://doi.org/10.1016/j.ccr.2015.06.005.

[48] Antolini E. Graphene as a new carbon support for low-temperature fuel cell catalysts. Appl Catal B Environ 2012;123–124:52–68. https://doi.org/10.1016/j.apcatb.2012.04.022.

[49] Wang H, Robinson JT, Diankov G, Dai H. Nanocrystal growth on graphene with various degrees of oxidation. J Am Chem Soc 2010;132:3270–1. https://doi.org/10.1021/ja100329d.

[50] Kushch SD, Kuyunko NS, Muradyan VE, Tarasov BP. Preparing hydrogenation catalysts via the simultaneous reduction of graphite oxide and platinum(IV). Russ J Phys Chem 2013;87:1798–803. https://doi.org/10.1134/S0036024413100117.

[51] Arbuzov AA, Mozhzhukhin SA, Volodin AA, Fursikov PV, Tarasov BP. Graphene-like nanostructures: synthesis and use for preparation of catalysts and hydrogen storage composites. Russ Chem Bull 2016;65:1893–901. https://doi.org/10.1007/s11172-016-1530-9.

[52] Klyuev MV, Arbuzov AA, Magdalinova NA, Kalmykov PA, Tarasov BP. Palladium-containing graphene-like material: synthesis and catalytic activity. Russ J Phys Chem 2016;90:1749–53. https://doi.org/10.1134/S0036024416090144.

[53] Bai J, Zhu Q, Lv Z, Dong H, Yu J, Dong L. Nitrogen-doped graphene as catalysts and catalyst supports for oxygen reduction in both acidic and alkaline solutions. Int J Hydrog Energy 2013;38:1413–8. https://doi.org/10.1016/j.ijhydene.2012.11.039.

[54] Arbuzov AA, Muradyan VE, Tarasov BP. Synthesis of graphene-like materials by graphite oxide reduction. Russ Chem Bull 2013;62:1962–6. https://doi.org/10.1007/s11172-013-0284-x.

[55] Førde T, Maehlen JP, Yartys VA, Lototsky MV H. Uchida. Influence of intrinsic hydrogenation/dehydrogenation kinetics on the dynamic behaviour of metal hydrides: a semi-empirical model and its verification. Int J Hydrog Energy 2007;32:1041–9.

[56] Mooij L, Dam B. Nucleation and growth mechanisms of nano magnesium hydride from the hydrogen sorption kinetics. Phys Chem Chem Phys 2013;15:11501–10.

[57] Rudman PS. Hydrogen-diffusion-rate-limited hydriding and dehydriding kinetics. J Appl Phys 1979;50(11):7195–9.

[58] Lototskyy M, Goh J, Davids MW, Linkov V, Khotseng L, Ntsendwana B, Denys R, Yartys V. Nanostructured hydrogen storage materials prepared by high-energy reactive ball

milling of magnesium and Ferrovanadium. Int J Hydrog Energy 2019;44:6687—701. https://doi.org/10.1016/j.ijhydene.2019.01.135.

[59] Liang X, Wang Y, Zheng H, Wu Z. X-ray absorption spectroscopy study on the thermal and hydrazine reduction of graphene oxide. J Electron Spectrosc Relat Phenom 2014;196:89—93. https://doi.org/10.1016/j.elspec.2013.10.011.

[60] Cahn JW. Transformation kinetics during continuous cooling. Acta Metall 1956;4:572—5.

[61] Stander CM. Kinetics of formation of magnesium hydride from magnesium and hydrogen. Z Physik Chem NF 1977;104:229—38.

[62] Denys RV, Riabov AB, Maehlen JP, Lototsky MV, Solberg JK, Yartys VA. *In situ* synchrotron X-ray diffraction studies of

hydrogen desorption and absorption properties of Mg and Mg-Mm-Ni after Reactive Ball Milling in hydrogen. Acta Mater 2009;57(13):3989—4000.

[63] Fernández JF, Sánchez CR. Rate determining step in the absorption and desorption of hydrogen by magnesium. J Alloy Compd 2002;340:189—98. https://doi.org/10.1016/S0925-8388(02)00120-2.

[64] Mao J, Guo Z, Yu X, Liu H, Wue Z, Ni J. Enhanced hydrogen sorption properties of Ni and Co-catalyzed MgH_2. Int J Hydrog Energy 2010;35:4569—75. https://doi.org/10.1016/j.ijhydene.2010.02.107.

[65] Luo FP, Wang H, Ouyang LZ, Zeng MQ, Liu JW, Zhu M. Enhanced reversible hydrogen storage properties of a Mg-In-Y ternary solid solution. Int J Hydrog Energy 2013;38:10912—8. https://doi.org/10.1016/j.ijhydene.2013.03.007.